Vortex Fusion and Giant Vortex States in Confined Superconducting Condensates

T. Cren, L. Serrier-Garcia, F. Debontridder, and D. Roditchev*

Institut des Nanosciences de Paris, Université Pierre et Marie Curie-Paris 6 and CNRS-UMR 7588, 4 place Jussieu, 75252 Paris, France

(Received 18 April 2011; published 23 August 2011)

In a direct scanning tunneling spectroscopy experiment we address the problem of the quantum vortex phases in strongly confined superconductors. The strong confinement regime is achieved in *in situ* grown ultrathin single nanocrystals of Pb by tuning their lateral size to a few coherence lengths. Upon an external magnetic field, the scanning tunneling spectroscopy revealed novel ultradense arrangements of single Abrikosov vortices characterized by an intervortex distance up to 3 times shorter than the bulk critical one. At yet stronger confinement we discovered the giant vortex phase; the spatial evolution of the excitation tunneling spectra in the cores of these unusual quantum objects was explored. We anticipate the giant vortex phase to be a common feature of other confined quantum condensates such as superfluids, Bose-Einstein condensates of cold atoms, etc.

DOI: 10.1103/PhysRevLett.107.097202 PACS numbers: 74.25.Ha, 74.25.Sv, 74.78.Na, 75.40.−s

When put in rotation, macroscopic quantum condensates develop a very peculiar collective response: They split into a huge number of small quantum tornadoes—vortices—that organize in a lattice [1]. The vortex currents circulate owing to the gradient of the condensate wave function $\Psi(\mathbf{r})$ that accumulates exactly 2π phase difference around each vortex core where $\Psi(\mathbf{r})$ vanishes. This general quantum phenomenon was observed in superconductors [2], superfluids [3], and Bose-Einstein condensates of ultracold atoms [4]. The confinement of quantum condensates to scales comparable to their characteristic coherence length should modify the vortex lattice, leading to novel vortex arrangements [5–9]. Moreover, new quantum objects—giant vortices—characterized by the phase accumulation $L \times 2\pi$, $L \geq 2$, were predicted to exist [8]. Until now the vortex confinement problem was addressed by transport and tunneling measurements [10,11], Bitter decoration [12], Hall magnetometry studies [13], and scanning Hall probe experiments [14], some giving evidence for the giant vortex. However, as these techniques do not probe the vortex *cores*, they rely on additional theoretical considerations to discriminate, for instance, between a dense cluster of L individual 2π vortices (a multivortex configuration) and a single $L \times 2\pi$ giant vortex. The experimental data accessing $\Psi(\mathbf{r})$ and thus observing the confined vortex configurations directly in real space are missing.

In this Letter we report a direct scanning tunneling microscopy and spectroscopy (STM/STS) experiment, revealing strong confinement effects on the vortex arrangements in extreme type II superconductors (see Supplemental Materials [15] for the method justification). The samples—atomically flat nanometer-sized single crystals of Pb—were *in situ* grown on undoped Si(111) [16]. The experiments were performed in an ultrahigh vacuum $P = (3–6) \times 10^{-11}$ mbar, and the magnetic field was applied perpendicular to the substrate. Mechanically sharpened Pt/Ir tips were used. In order to resolve fine spectroscopic features, the STM/STS experiments were conducted at 320 mK, i.e., at $T \approx T_c/20$ [17]. Three crystals were selected for this STM/STS study, denoted $N1$, $N2$, and $N3$ (Fig. 1). Their lateral dimensions are $D_{N1} \approx 140$ nm, $D_{N2} \approx 80–140$ nm, $D_{N3} \approx 80$ nm and heights $h_{N1} \approx 2.8$ nm, $h_{N2} = h_{N3} \approx 2.3$ nm, i.e., 10 and 8 single atomic layers of Pb in (111) direction. Importantly, due to the atomic lattice mismatch, the Pb-Si interface is

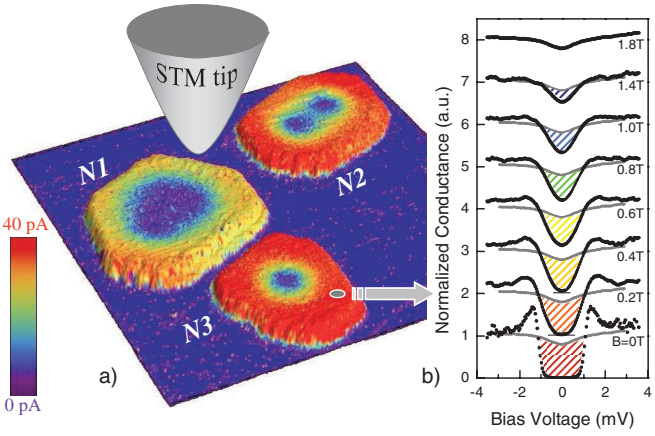

FIG. 1 (color). Response of studied confined superconducting condensates to the magnetic field. (a) 250 nm × 200 nm constant current topographic STM image of three selected islands. The superposed color-coded gapped area map at 0.8 T visualizes the superconducting regions in red, the normal state vortex cores appearing in dark blue. (b) Local tunneling conductance spectra $dI/dV(V)$ acquired at the periphery of the smallest crystal $N3$ at different magnetic fields. The spectra are presented normalized to unity at 50 nS (set point $I_0 = 250$ pA, $V_0 = 5$ mV) and shifted for clarity. The gapped area is hashed; the colors respect the rainbow pallet (see Supplemental Materials [15] for further details).

disordered [16]. This strongly limits the electron mean free path in Pb crystals to $l \approx (2\text{–}3)h = 5\text{–}8$ nm [18] and thus plays an important role in their superconducting properties. Indeed, the coherence length and the penetration depth for such thin and diffusive superconductors take the effective values $\xi_{\mathrm{eff}} \simeq \sqrt{\xi_0 l}$ and $\Lambda_{\mathrm{eff}} \simeq \lambda_{\mathrm{eff}}^2/h$, with $\lambda_{\mathrm{eff}} \simeq \lambda_0\sqrt{\xi_0/l}$, where $\xi_0 = 80$ nm and $\lambda_0 \simeq 50$ nm are, respectively, the coherence length and the penetration depth in bulk Pb [19]. For our islands we get $\xi_{\mathrm{eff}} \approx 25$ nm and $\Lambda_{\mathrm{eff}} \approx 12\,000$ nm. Thus, the situation $l \ll \xi_{\mathrm{eff}} \ll \Lambda_{\mathrm{eff}}$ is that of an extreme type II superconductor ($\kappa = \lambda_{\mathrm{eff}}/\xi_{\mathrm{eff}} \approx 8$) in the diffusive limit. The ratio between lateral dimensions D_i and ξ_{eff} defines the expected strong confinement conditions $D_i \approx (3\text{–}6)\xi_{\mathrm{eff}} \ll \Lambda_{\mathrm{eff}}$. Moreover, the condition $h \ll D_i \ll \Lambda_{\mathrm{eff}}$ implies that, although strong screening supercurrents may circulate in the island, their diamagnetic (Meissner) effect is weak; i.e., the applied magnetic field fully penetrates the sample $B \simeq B_{\mathrm{app}}$ [20]. Consequently, no mutual magnetic influence is expected between neighboring islands.

Our main finding is illustrated in Fig. 1 where we show a color-coded spectroscopic map of the situation in our confined superconductors subject to a magnetic field $B_{\mathrm{app}} = 0.8$ T. Here the rainbow pallet represents the gapped area (GA) in the local tunneling conductance spectra and corresponds to the local strength of superconducting condensate (see Supplemental Materials [15] for further details): It varies from red (strong superconductivity) to dark blue-violet (normal state). A single vortex is observed in the smallest island $N3$: Its normal core is directly visualized as a small blue spot. Two separate 2π vortices occupy the elongated $N2$: Their individual cores are clearly resolved. However, only one large object is observed in the crystal $N1$ in which, could the confinement effects be neglected, three separated individual vortices would exist. The core of this object appears in dark blue, indicating that the superconductivity is fully suppressed there.

In order to identify the observed quantum phenomenon, we explored the evolution of the superconductivity in the islands with the magnetic field (Fig. 2). At zero magnetic field, the GA map shows a spatially homogeneous superconducting condensate to exist in all nanoislands, characterized by a well-pronounced superconducting gap and thus appearing in red (see Supplemental Materials [15] for further details). There the individual tunneling $dI/dV(V)$ spectra reveal a conventional superconductivity with a gap $\Delta = 1.2$ meV [Fig. 1(b), lowest curve].

At 0.2 T the GA map in Fig. 2 shows no vortices: The superconducting gap is observed everywhere on the islands, evidencing the Meissner ($L = 0$) state. However, as compared to the zero-field map, the color of the islands evolves from red to orange, reflecting the reduction of the condensate strength, the periphery of islands being more affected. In fact, as the magnetic field is set on, the

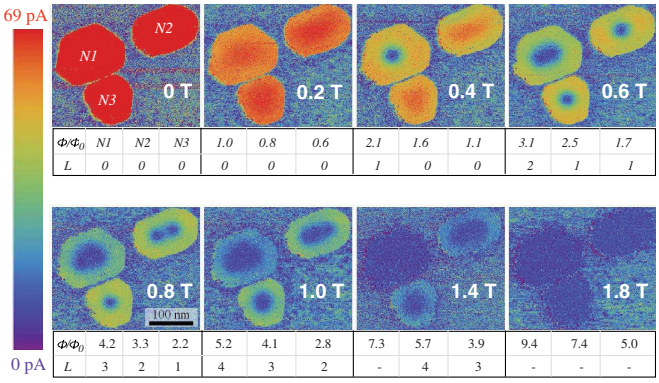

FIG. 2 (color). Overall evolution of the confined condensates in the magnetic field (color-coded GA maps). The magnetic flux Φ_i crossing each island (in units of Φ_0) and the winding factors L_i are given for each value of the applied magnetic field (for the details of calculations of Φ_i and L_i see Supplemental Materials [15]).

condensate is put in rotation: The screening currents weaken the condensate via depairing effect and affect its excitation spectrum [18,21,22]. The distribution of supercurrents is described by the sum of two contributions $\vec{j}_s = -\frac{\hbar e}{m}|\Psi|^2(\vec{\nabla}\varphi + \frac{2e}{\hbar}\vec{A})$, where $\Psi = |\Psi|e^{i\varphi}$ [23]. In the Meissner phase the vortices are absent, and considering a cylindrical geometry, the superconducting wave function has a constant phase $\vec{\nabla}\varphi = \vec{0}$ in the London gauge $\vec{A} = \frac{1}{2}\vec{B} \wedge \vec{r}$. The Meissner supercurrents $\vec{j}_s = -\frac{\hbar e}{m}|\Psi|^2\frac{2e}{\hbar}\vec{A}$ circulate owing to the nonzero value of the vector potential $\vec{A}$ whose amplitude is proportional to the distance r from the center: $A = \frac{1}{2}B_{\mathrm{app}}r$. It results in the rise of the screening supercurrents towards the cylinder periphery $j_s \propto B_{\mathrm{app}}r$, as visualized in Fig. 2. The kinetic energy E_k of these currents strongly depends on lateral size D of the islands ($E_k \propto D^4B_{\mathrm{app}}^2$ in a thin cylinder); it is strongly concentrated at the periphery of the cylinder: $\partial E_k/\partial r \propto r^3$. Therefore, in a rising field the depairing currents would rapidly destroy the superconductivity from the periphery to the center.

The vortex penetration allows the confined condensate to survive: The vortex supercurrents flow in the opposite direction with respect to the Meissner supercurrents and interfere destructively, thus significantly reducing the kinetic energy of the rotating condensate [18]. Indeed, the GA map at 0.4 T (Fig. 2) shows a single vortex to appear in the crystal $N1$ ($L = 1$), which is penetrated here by a magnetic flux $2.1\Phi_0$, where Φ_0 is the flux quantum $\Phi_0 = h/2e$. The crystals $N2$ and $N3$, crossed by a flux $1.6\Phi_0$ and $1.1\Phi_0$, respectively, remain in the Meissner phase. They reach the single vortex phase $L = 1$ at higher fields (Fig. 2, GA map at 0.6 T).

As the field increases further, the GA maps in Fig. 2 reveal novel intriguing vortex configurations, evolving till the normal state is achieved in each crystal. In order to get a

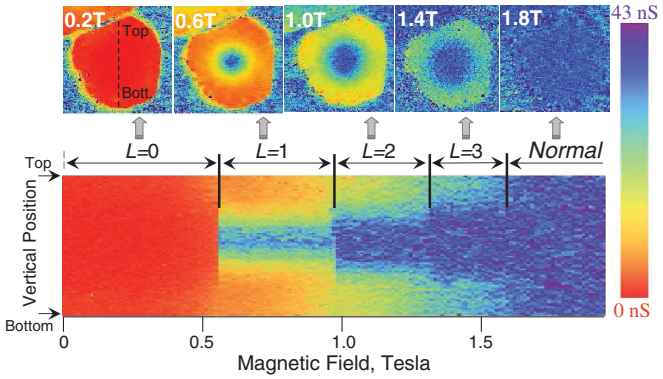

FIG. 3 (color). Giant vortex configurations in the crystal $N3$. Bottom: Color-coded diagram of ZBC values vs magnetic field taken over a line crossing the island $N3$ center. Abrupt transitions separate the phases of different vorticity L. Top: ZBC maps of corresponding configurations. Dashed line: The scanning line along which the ZBC-field diagram was acquired.

deeper insight into these phases we first focus on the field evolution of the condensate confined in the smallest crystal $N3$. In Fig. 3 we present a color-coded diagram of zero-bias conductance (ZBC) vs magnetic field taken over a line crossing the island center (depicted as a dashed line) [24]. The diagram shows a series of abrupt steplike transitions which are identified as separating the states with different vorticity L. Precisely, until 0.6 T the island remains in the Meissner state ($L = 0$), in agreement with the GA maps in Fig. 2. At 0.6 T the first vortex appears at the center; it is clearly identified by its normal state core (dark blue). This single vortex state lasts until 0.9 T. The $L = 2$ phase occurs at $0.9\ \mathrm{T} < B_{\mathrm{app}} < 1.3\ \mathrm{T}$, followed by the $L = 3$ state ($1.3\ \mathrm{T} < B_{\mathrm{app}} < 1.6\ \mathrm{T}$). Remarkably, in the $L = 2$ phase both the ZBC map in Fig. 3 and GA map in Fig. 2 at 1.0 T show a single round object located at the crystal center, instead of two individual vortices. The size of this object is larger than that of a single vortex core. In the $L = 3$ phase a similar phenomenon is observed: Instead of 3 separated vortices, the map at $B_{\mathrm{app}} = 1.4$ T shows the suppression of superconductivity in one single region. The straightforward conclusion is that here two (three) individual vortex cores are merged to form a single 4π (6π) giant vortex.

Although in $N3$ the giant vortex state sets in already at $L = 2$, in larger islands $N1$ and $N2$ where the confinement is weaker, the situation is more subtle; the analysis of the ZBC profiles presented in Fig. 4 is required to identify the observed configurations. First, the single vortex profiles in the $L = 1$ state were studied and found to be similar in all crystals. The best fits (thin solid lines) within Ginzburg-Landau theory [25] were obtained for $\xi_{N1} = 30$ nm, $\xi_{N2} = 27$ nm, $\xi_{N3} = 28$ nm, in agreement with our initial rough estimate for ξ_{eff} (25 nm). These profiles show the existence of a singular location where the superconductivity is fully suppressed; starting from this singular point the superconducting gap opens almost linearly on the scale of

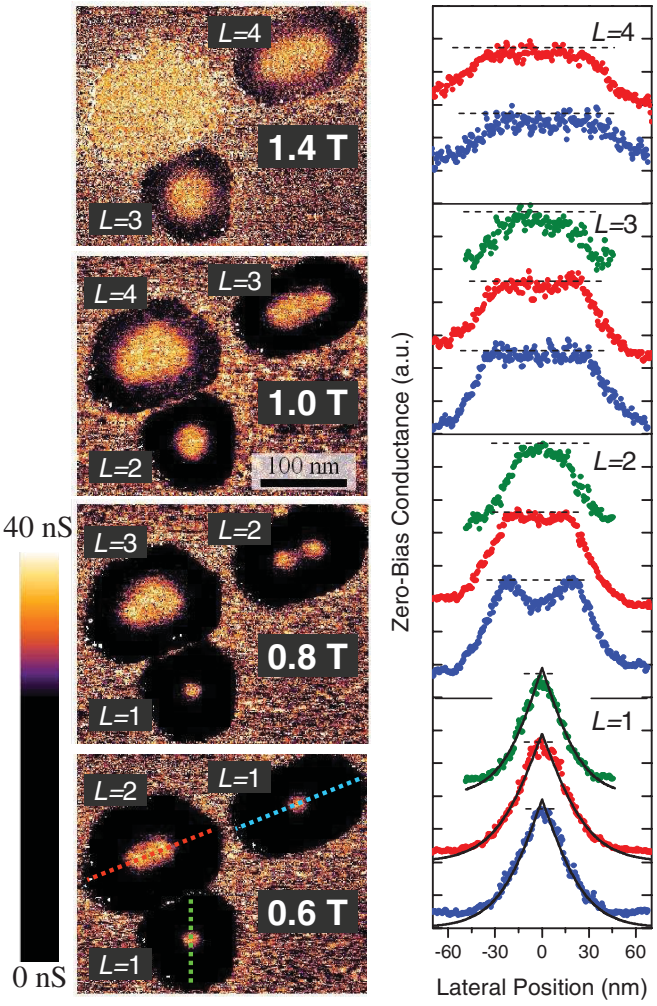

FIG. 4 (color). Shapes and profiles of confined vortex phases. Left panel: ZBC maps revealing the extension of the vortex cores in different situations. The locations characterized by a superconducting gap are intentionally saturated in black; the cores of individual 2π vortices appear as small bright spots (see the color bar). With the same contrast, the $L > 2$ phases are revealed as extended regions. Right panel: ZBC profiles of different vortex configurations recorded along the lines presented in color in the ZBC map. From bottom to top: $L = 1$ state—the profiles of single 2π vortices (dots) and their fits by the Ginzburg-Landau formula [25] (thin solid lines); $L = 2$ state—two close vortex cores in the crystal $N2$ at 0.8 T appear separate (blue dots), at shorter distance (34 nm) the cores merge (crystal $N1$ at 0.6 T—red dots), and there is a bell-shaped profile of the 4π giant vortex core in $N3$ at 1.0 T (green dots); the $L = 3$ and $L = 4$ phases are discussed in the text. Horizontal dashed lines correspond to the ZBC in the normal state.

ξ_{eff}. This is exactly the behavior theoretically expected for vortex cores in the dirty limit; it is also in agreement with previous experimental findings [25]. The $L = 2$ phase in the elongated $N2$ is a multivortex configuration composed of two 2π vortices: At 0.8 T the cores are separated by 39 nm ($\approx 1.4\xi_{N2}$). The confinement is so strong that the intervortex distance here is 2 times shorter than

the minimum value possible in bulk superconductors ($a_{B_{c2}} \approx 2.8\xi_{\text{eff}}$, achieved at the second critical field B_{c2}). The corresponding saddle-shaped ZBC profile evidences the suppression of the order parameter at two singular points, but also the weakening of the superconductivity in between. The $L = 2$ state in $N1$ is also a multivortex configuration composed of two close 2π vortices characterized, at 0.6 T, by an extremely short vortex-vortex distance, 34 nm ($\approx 1.1\xi_{N1}$), i.e., 2.5 times shorter than $a_{B_{c2}}$. The vortex cores strongly overlap: The ZBC profile becomes completely flat between the cores, as the gap is no more observed there.

The central part of the $L = 2$ multivortex profiles in $N1$ and $N2$ is thus strikingly different from the 4π giant vortex profile in $N3$: The latter has a characteristic bell-like shape (Fig. 4, green dots, see also Fig. 2 in the Supplemental Materials [15]). The difference certainly originates from the specific topology of Ψ in each case: In the multivortex phases there are L spatially separated ($\approx \xi_{\text{eff}}$) singular points where $|\vec{\nabla}\varphi| \to \infty$, while in the giant vortex configuration there is only one such singular location. The observed round profile of the giant vortex is intimately related to its phase gradient $|\vec{\nabla}\varphi| = L/r$ [5], i.e. L times stronger than around a 2π vortex. Elementary calculations within Ginzburg-Landau theory show that in the vicinity of the core center the superconducting order parameter evolves as $|\Psi| \propto r^L$ [26]. Thus, the observed V-shaped profiles of single 2π vortices and the bell-shaped one of the 4π giant vortex are in qualitative agreement with this prediction (for further details see Supplemental Materials [15]).

At $L = 3$ the giant vortex core profile in $N3$ is bell-shaped, yet it is flatter than at $L = 2$, consistent with the expected $|\Psi| \propto r^3$ dependence. To the contrary, the profiles in $N1$ and $N2$ at $L = 3$, completely flat in their central part, are jagged at the edges; therefore, we identify them as superdense ($\approx \xi_{\text{eff}}$) multivortex configurations. At $L = 4$ the ZBC profiles in $N1$ and $N2$ are consistent with the giant vortex state. However, a tiny difference between a slightly rounded giant vortex core ($|\Psi| \propto r^4$) and a completely flat profile of a superdense multivortex phase becomes difficult to discriminate experimentally. Note that in the limit of large L the two configurations should become undistinguishable.

The observed vortex phase diagram has an important general issue. Until now the giant vortex was mostly considered as due to a balance between the condensation and magnetic energies, the second term being due to the Meissner diamagnetism generated by moving charged Cooper pairs. Consequently, the giant vortex was thought as a sort of oddity, specific to superconductivity. In our extreme type II confined case, $\xi_{\text{eff}} \lesssim D_i \ll \Lambda_{\text{eff}}$, the magnetic energy does not play any significant role in the energy balance. Our experiments prove that the confinement is sufficient alone to stabilize the observed superdense multivortex and giant vortex phases, which should also exist in other strongly confined neutral quantum condensates (cold atoms, superfluids, etc.), and thus are common quantum features.

In conclusion, strong vortex confinement effects were studied in atomically perfect Pb nanocrystals by STM/STS at 0.3 K. In these extreme type II superconductors an unexpected superdense multivortex phase was discovered; it precedes the giant vortex phase which was directly observed. Giant vortex cores were revealed for the first time and showed a r^L spatial dependence.

This work was supported by grants from the French National Agency for Research (ANR, project GAPSUPRA) and by the CNRS (L. S.-G.). The authors thank Ch. Brun for critical comments and precious help in the preparation of the manuscript. We are also grateful to A. Buzdin for fruitful discussion.

*dimitri.roditchev@insp.jussieu.fr

[1] A. A. Abrikosov, Sov. Phys. JETP **5**, 1174 (1957); Nobel Lecture (2003), http://nobelprize.org/nobel_prizes/physics/laureates/2003/abrikosov-lecture.pdf.
[2] U. Essmann and H. Trauble, Phys. Lett. **24A**, 526 (1967).
[3] E. J. Yarmchuk, M. J. V. Gordon, and R. E. Packard, Phys. Rev. Lett. **43**, 214 (1979).
[4] J. R. Abo-Shaeer, C. Raman, J. M. Vogels, and W. Ketterle, Science **292**, 476 (2001).
[5] D. Saint-James, Phys. Lett. **15**, 13 (1965).
[6] H. J. Fink and A. G. Presson, Phys. Rev. **151**, 219 (1966).
[7] P. S. Deo, V. A. Schweigert, F. M. Peeters, and A. K. Geim, Phys. Rev. Lett. **79**, 4653 (1997).
[8] V. A. Schweigert, F. M. Peeters, and P. S. Deo, Phys. Rev. Lett. **81**, 2783 (1998).
[9] L. F. Chibotaru, A. Ceulemans, V. Bruyndoncx, and V. V. Moshchalkov, Nature (London) **408**, 833 (2000).
[10] L. F. Chibotaru, A. Ceulemans, V. Bruyndoncx, and V. V. Moshchalkov, Phys. Rev. Lett. **86**, 1323 (2001).
[11] A. Kanda, B. J. Baelus, F. M. Peeters, K. Kadowaki, and Y. Ootuka, Phys. Rev. Lett. **93**, 257002 (2004).
[12] I. V. Grigorieva *et al.*, Phys. Rev. Lett. **99**, 147003 (2007).
[13] A. K. Geim *et al.*, Nature (London) **390**, 259 (1997).
[14] R. B. G. Kramer, A. V. Silhanek, J. Van de Vondel, B. Raes, and V. V. Moshchalkov, Phys. Rev. Lett. **103**, 067007 (2009).
[15] See Supplemental Material at http://link.aps.org/supplemental/10.1103/PhysRevLett.107.097202 for the method justification, the calculation of the magnetic flux penetrating each sample (as it appears in Fig. 2), and the detailed profiles of giant vortex cores $L = 2$ and $L = 3$.
[16] K. Budde, E. Abram, V. Yeh, and M. C. Tringides, Phys. Rev. B **61**, R10602 (2000).
[17] C. Brun *et al.*, Phys. Rev. Lett. **102**, 207002 (2009).
[18] T. Cren *et al.*, Phys. Rev. Lett. **102**, 127005 (2009).
[19] M. Tinkham, Phys. Rev. **129**, 2413 (1963).

[20] E. H. Brandt and J. R. Clem, Phys. Rev. B **69**, 184509 (2004).
[21] K. Maki and P. Fulde, Phys. Rev. **140**, A1586 (1965).
[22] A. Anthore, H. Pothier, and D. Esteve, Phys. Rev. Lett. **90**, 127001 (2003).
[23] *Superconductivity of Metals and Alloys*, edited by P. G. de Gennes (W. A. Benjamin Inc., New York, 1966).
[24] To record the ZBC diagram, the local tunneling spectra were continuously acquired along a line (the dashed line in Fig. 3), while slowly sweeping up the magnetic field (≈ 5 mT/line).
[25] M. R. Eskildsen *et al.*, Phys. Rev. Lett. **89**, 187003 (2002).
[26] *Type II Superconductivity*, edited by D. Saint-James, G. Sarma, and E. J. Thomas (Pergamon Press, Oxford, 1969).